Hyperfine Interact (2010) 198:273–293
DOI 10.1007/s10751-010-0193-4

Microscopic ^{57}Fe electric-field-gradient and anisotropic mean-squared-displacement tensors: ferrous chloride tetrahydrate

James N. Bull · Christopher M. Fitchett · W. Craighead Tennant

Published online: 18 November 2010

Abstract This paper reports the determination of the electric-field-gradient and mean-squared-displacement tensors in ^{57}Fe symmetry-related sites of $\bar{1}$ Laue class in monoclinic $FeCl_2.4H_2O$ at room temperature by single-crystal Mössbauer spectroscopy. Contrary to all previous work, the mean-squared-displacement matrix (tensor), <msd>, is not constrained to be isotropic resulting in the determination of physically meaningful estimates of microscopic (local) electric-field gradient (efg) and <msd> tensors. As a consequence of anisotropy in the <msd> tensor the absorber recoilless fractions are also anisotropic. As expected of a low-symmetry site, Laue class $\bar{1}$ in this case, no two principal axes of the efg and <msd> tensors are coaxial, within the combined errors in the two. Further, no principal direction of the efg tensor seems related to bond directions in the unit cell. Within error, and in agreement with an earlier study of sodium nitroprusside, it appears that the <msd> tensor principal directions lie close to the crystallographic axes suggesting that they are determined by long wavelength (phonon) vibrations in the crystal rather than by approximate local symmetry about the ^{57}Fe nucleus. Concurrent with the Mössbauer measurements, we determined as part of a new X-ray structural determination, precise atomic displacement parameters (ADPs) leading to an alternative determination of the <msd> matrix (tensor). The average of the eigenvalues of the Mössbauer-determined <msd> exceeds that of the average of the X-ray-determined eigenvalues by a factor of around 2.2. Assuming isotropic absorber recoilless fractions leads to substantially the same (macroscopic) efg tensor as had been determined in earlier work. Taking $\frac{1}{3}\times$ the trace of the anisotropic absorber recoilless fractions leads to an isotropic value of 0.304 in good agreement with earlier single crystal studies where isotropy was assumed.

J. N. Bull · C. M. Fitchett · W. C. Tennant (✉)
Department of Chemistry, University of Canterbury, Private Bag 4800,
Christchurch, New Zealand
e-mail: craig.tennant@canterbury.ac.nz

Keywords Mössbauer spectroscopy · Single crystals · Symmetry-related sites · Microscopic and macroscopic efg tensors · Atomic displacement parameters · Lamb-Mössbauer factors

1 Introduction

There have been a number of papers that have reported the determination of the electric-field-gradient (efg) tensor at the Fe^{2+} site in $FeCl_2.4H_2O$ (here abbreviated to FCL) single crystals by Mössbauer spectroscopy. The earliest, and probably still the most referenced paper, is that of Peter Zory [1]. Zory, for the first time, derived algebraic expressions for the orientation dependence of the quadrupole doublet line intensities in the principal axis system of the efg tensor for a low symmetry case when the asymmetry parameter, η, is non-zero. He utilized these equations to obtain the efg for FCL from measurements of area ratios in seven single crystal orientations including the three orthogonal orientations of the laboratory axis system, $\mathbf{c} \times \mathbf{b}$, $\mathbf{c}$, $\mathbf{b}$ of the monoclinic $P2_1/c$ space group of FCL. Additionally, Zory correctly inferred the sign of the quadrupole splitting as positive and an anisotropy in the absorber recoilless fraction, f_{abs}.

Not recognized in the above study, as first pointed out by Zimmermann [2], is that the efg obtained by Zory was in fact a macroscopic tensor arising from the composite quadrupole doublet of two symmetry-related Fe sites in the monoclinic unit cell; the sites are related by a rotation π about the crystallographic-unique axis **b**. Zimmermann [2] determined the macroscopic efg in an intensity–tensor formalism and determined the limits of the manifold of solutions of the efgs of the two contributing microscopic (or, local) efgs. Both the Zory and Zimmermann determinations assumed the "thin crystal" approximation. That is, thickness-dependent polarization of the gamma radiation by the single crystal absorber was neglected. Gibb [3] and Spiering and Vogel [4] re-determined the macroscopic efg of FCL at 300 K, each making thickness corrections including polarization. Gibb in addition used polarized source (i.e., magnetically perturbed) measurements and obtained e^2qQ ($= e\,Q\,P_{\hat{z}\hat{z}}$ in the nomenclature of this paper; note that, throughout, we shall use the notation $T_{\hat{\alpha}\hat{\alpha}}$ to denote a principal value of a matrix $\mathbf{T}$) positive in agreement with Zory [1] and independent measurements of Grant et al. [5]. Ono et al. [6] also inferred a positive value from measurements below the Néel temperature. Gibb deduced additionally a recoilless fraction, $f_{abs} = 0.28 \pm 0.02$ (assumed isotropic) in agreement with the value $f_{abs} = f_{powder} = 0.29$ determined by Kerler and Neuwirth [7] and assumed by Spiering and Vogel [4]. In all of these studies isotropic thermal nuclear displacements were assumed.

In the work here reported we have attempted to measure the mean-squared-displacements (msds) of the Fe^{2+} directly from our Mössbauer experiments and obtain thereby estimates of anisotropy in the related absorber recoilless fractions—assuming that is, that such anisotropy is sufficient to be measurable. In a recent related publication we used similar procedures to obtain values for both the efg and <msd> tensors in ferrous ammonium sulphate hexahydrate [8] with the assumptions: "generally the <msd> tensor will be anisotropic and …., from [9], intensity calculations involving an anisotropic <msd> tensor can, *in favourable circumstances*, resolve the ambiguity resulting from two symmetry-related Fe sites". By *favourable* it was implied that the anisotropy in the <msd> tensor is adequate. In retrospect,

the foregoing may be a simplification and a number of caveats need be stated as follows. To obtain the <msd> tensor from Mössbauer measurements one needs to be able to obtain good estimates of the total intensities, expressed as dimensionless quantities, of the two lines of the quadrupole doublet. As pointed out by Grant, Housley and Gonser [10] in their classic work on sodium nitroprusside, the <msd> is a symmetric tensor of rank 2 with, generally, six independent parameters and usually many more orientation-dependent spectra are required for its determination than for the second-rank traceless efg tensor. This is because the <msd> generally makes a much smaller contribution to the spectrum than the efg tensor. The measurements, to be later-described, were restricted to a cone of orientations obtained by rotating the crystal about the perpendicular to the bc plane oriented at 45° to the gamma beam; the bc plane is the natural growth habit of the crystal and crystals are able readily to be polished parallel to this plane for Mössbauer experiments. Although this provides readily a large number of general orientations it is still, as we shall see later, inadequate to describe fully the <msd> tensor. Further, use of X-ray determined atomic-displacement parameters (ADPs) together with earlier efg tensor determinations to obtain expected angular dependences of reduced intensities and total intensities of a quadrupole doublet lines may be questioned since, to our knowledge, no quantitative relationship between X-ray and Mössbauer determined msds has been established.

We shall nevertheless follow, initially at least, Bull et al. [8] in simulating the expected angular dependence of the two quantities above from ADPs measured in this laboratory from a precise new X-ray structure determination, and the 300 K macroscopic intensity tensor reported by Spiering and Vogel [4]. In fact we performed a number of simulations within the limits of the possible manifold of solutions of the macroscopic efg and <msd> tensors in order to assess how these variations affect the plots obtained; one such set of plots will be presented. We do not know how the magnitudes of the Mössbauer <msd> tensor will vary from those expected from X-ray measurements, although all measurements to date indicate ~50% or greater magnitudes for the Mössbauer-determined values. In simplest terms, as discussed in the next section, one might expect, assuming similar scattering mechanisms in the two experiments that the msd will vary as the inverse square of the wavelength. With this assumption a factor $\lambda^2(\mathrm{Fe})/\lambda^2(\mathrm{Mo}) = (0.8602)^2/(0.7107)^2 = 1.465$ might be expected but this appears, from the few Mössbauer measurements available to be, at best, an approximation. Nevertheless, we shall see that these prediction plots give a sufficiently good representation of the experimentally obtained Mössbauer plots to match confidently crystallographic orientations, to obtain reasonable first estimates of msds (and hence f_{abs} values) and indeed anisotropies in these quantities. We then proceed to a more complete analysis of the data using essentially the methods first set out by Grant et al. [10], further detailed by Zimmermann [11] and used by ourselves [8] to obtain physically sound microscopic efg and <msd> tensors for ferrous ammonium sulphate hexahydrate.

2 Theory

2.1 Crystallography and intensity–tensor relationships

FCL crystallizes in the monoclinic space group $P2_1/c$ with two crystallographically equivalent sites for Fe per unit cell each with point-group symmetry 1 (Laue class $\bar{1}$)

and related by a rotation π about the crystallographic-unique axis, **b**. As part of this work a room temperature (295 K) X-ray structure (Mo K_α radiation, $\lambda = 0.7107$ Å) was determined on a small single crystal obtained by re-crystallizing an "Analar" material. For space group $P2_1/c$ the determined cell parameters were, in units Å, $a = 5.8765$ (3), $b = 7.1100$ (3), $c = 8.4892$ (5) and $\beta = 111.096$ (1)°. The anisotropic atomic displacement parameters for Fe referred to the crystal axis system were, in units Å^2, $U_{11} = 0.00945$ (19), $U_{22} = 0.01449$ (19), $U_{33} = 0.00937$ (19), $U_{12} = 0.00125$ (6), $U_{13} = 0.00386$ (13), and $U_{23} = 0.00030$ (7). The R factor was 1.51% for 927 reflections. The present re-determination is in agreement, apart from one erroneous Fe-O bond length, with the structure reported by Penfold and Grigor [12] and later confirmed by Meunier-Piret and Van Meersche [13]. A further neutron diffraction study by Verbist et al. [14] found that, by treating the two iron sites differently a better R factor was obtained as well as claimed evidence of a lowering of the space-group symmetry from $P2_1/c$ to $P2_1$. Our precise X-ray diffraction study, details of which are available [15], gave a significantly better R factor, determined all H atom positions and confirmed the $P2_1/c$ space group.

For the experiments reported here we followed all earlier works [1, 3, 4] in choosing an orthogonal set of axes (**a**′, **c**, **b**) = (**c** × **b**, **c**, **b**); here a, b and c are the crystallographic axes. We shall require a set of orthogonalized displacement parameters, U^C_{ij} (in units Å^2 = 10^{-16} cm^2), referred to the laboratory axes ($\mathbf{x}_0$, $\mathbf{y}_0$, $\mathbf{z}_0$) = (**a**′, **c**, **b**). From the above X-ray results one obtains the matrix **U** of atomic displacement parameters that can be orthogonalized to $\mathbf{U}^{\mathrm{C}}$ via

$$\mathbf{U}^{\mathrm{C}} = \mathbf{A}\mathbf{U}\mathbf{A}^{\mathrm{T}} \tag{1}$$

Where T = transpose and, from Trueblood et al. [16]

$$\mathbf{A} = \begin{pmatrix} \mathrm{a} & 0 & \mathrm{c}\cos\beta \\ 0 & \mathrm{b} & 0 \\ 0 & 0 & \mathrm{c}\sin\beta \end{pmatrix} \begin{pmatrix} \mathrm{a}^* & 0 & 0 \\ 0 & \mathrm{b}^* & 0 \\ 0 & 0 & \mathrm{c}^* \end{pmatrix}$$

where the symbol * denotes the reciprocal-space unit cell parameter. The matrix **U** and its transform $\mathbf{U}^{\mathrm{C}}$ are for FCL

$$\mathbf{U} = \begin{pmatrix} 0.00945 & 0.00125 & 0.00386 \\ 0.00125 & 0.01449 & 0.00030 \\ 0.00386 & 0.00030 & 0.00937 \end{pmatrix} \text{ and } \mathbf{U}^{\mathrm{C}} = \begin{pmatrix} 0.00906 & 0.00122 & 0.00052 \\ 0.00122 & 0.01449 & 0.00030 \\ 0.00052 & 0.00030 & 0.00937 \end{pmatrix} \tag{2}$$

It should be noted that matrix $\mathbf{U}^{\mathrm{C}}$ is identical to the so-called probability covariance matrix that can be obtained independently via programme ORTEP [17].

The required mean-squared-displacement matrix, ⟨**msd**⟩ has corresponding elements, defined in terms of dimensionless quantities

$$\langle msd \rangle_{ij} = k^2 U^C_{ij} \tag{3}$$

where, for either the X-ray or Mössbauer experiments, $k^2 = 4\pi^2/\lambda^2$, λ being the wavelength of the particular radiation (0.8602 Å and 0.7107 Å respectively for ^{57}Fe

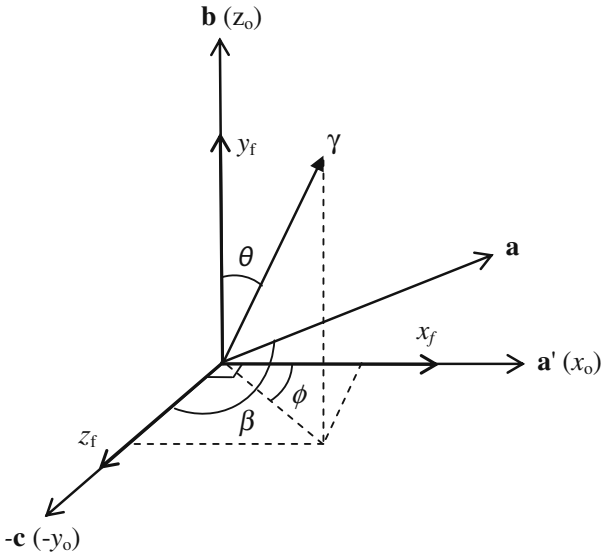

Fig. 1 Relationships between the crystal, (x_f, y_f, z_f), and laboratory, (x_0, y_0, z_0) coordinate frames

and Mo K_α radiations) and $U_{ij}^C s$ are displacements along wavevector **k**. For the X-ray case one obtains $k^2 = 78.1605 \times 10^{16}$ cm^{-2} leading to

$$\langle \mathbf{msd} \rangle_f = \begin{pmatrix} 0.70804 & 0.09568 & 0.04083 \\ 0.09568 & 1.13255 & 0.02345 \\ 0.04083 & 0.02345 & 0.73236 \end{pmatrix} \tag{4}$$

for the msd matrix referred to the crystal Cartesian coordinates (x_f, y_f, z_f) of Fig. 1. To transform to the orthogonal axes (x_0, y_0, z_0) chosen as the "laboratory" set, one must perform a $\pi/4$ clockwise rotation about axis **a**′ of Eq. 3. This leads to

$$\langle \mathbf{msd} \rangle = \begin{pmatrix} 0.70804 & 0.04083 & -0.09568 \\ 0.04083 & 0.73236 & -0.02345 \\ -0.09568 & -0.02345 & 1.13255 \end{pmatrix} \tag{5}$$

in the laboratory axis system. It is the matrix $\langle \mathbf{msd} \rangle$ of dimensionless quantities corresponding to Eq. 5 that we shall endeavor to determine by Mössbauer for FCL.

For each crystal orientation, i, described by the spherical polar pair (θ_i, ϕ_i), one can calculate the scalar quantity $\langle r^2 \rangle_i$ given by

$$\langle r^2 \rangle_i = \begin{pmatrix} \sin\theta_i \cos\phi_i & \sin\theta_i \sin\phi_i & \cos\theta_i \end{pmatrix} \begin{pmatrix} \langle xx \rangle & \langle xy \rangle & \langle xz \rangle \\ \langle xy \rangle & \langle yy \rangle & \langle yz \rangle \\ \langle xz \rangle & \langle yz \rangle & \langle zz \rangle \end{pmatrix} \begin{pmatrix} \sin\theta_i \cos\phi_i \\ \sin\theta_i \sin\phi_i \\ \cos\theta_i \end{pmatrix} \tag{6}$$

where $\langle xx\rangle$, $\langle xy\rangle$, ... are the (dimensionless) components of matrix $\langle \mathbf{msd}\rangle$ given in Eq. 5. It follows, in terms of (3) and (6), that the recoilless fraction, f_i, is given by

$$f_i = \exp\left(-\langle r^2\rangle_i\right) \tag{7}$$

Following [8] we shall express the efg tensor in the Zimmermann [2] traceless intensity–tensor formalism (here designated **P**) where, in addition to the requirement of zero trace, the following invariant holds

$$P_{zz}^2 + \frac{1}{3}(P_{xx} - P_{yy})^2 + \frac{4}{3}\left(P_{xy}^2 + P_{xz}^2 + P_{yz}^2\right) = \frac{1}{16} \tag{8}$$

We shall use the macroscopic efg data of Spiering and Vogel [4] that in the Zimmermann formalism may be expressed as

$$\mathbf{P} = \begin{pmatrix} -0.0755 & \sim 0 & P_{xz} \\ \sim 0 & 0.1470 & P_{yz} \\ P_{xz} & P_{yz} & -0.0715 \end{pmatrix} \tag{9}$$

From (8) we obtain the manifold of possible solutions bound by $P_{xz}^2 + P_{yz}^2 = 0.03066$. We shall examine simulations using the <msd> matrix from (5) together with one or other of three limiting cases for the P matrix: (1) $P_{xz} = 0$ when $P_{yz} = \pm 0.1751$ (2) $P_{yz} = 0$ when $P_{xz} = \pm 0.1751$ (3) $P_{xz} = P_{yz} = \pm 0.1238$. We discuss these simulations in a later section.

2.2 The goniometer system

FCL crystallizes most frequently as flat plates containing both the b and c crystallographic axes. In this work we collected single-crystal data by rotating the crystal about the perpendicular (the vector $\mathbf{a}'$) to the bc plane on a single-circle goniometer inclined at 45° to the gamma-beam direction. The beam then traces out a right-circular cone in the crystal where the measured directions lie on the surface of the cone; a full rotation of 2π is required (generally) to obtain a repeat spectrum. For rotation about $\mathbf{a}'$ ($\theta = \pi/2, \phi = 0$) in the laboratory axis system, the rotation of a vector on the cone surface lying initially along $\theta = \pi/4, \phi = 0$ by angle ε is given by [18] (p.87),

$$\mathbf{D}(-\pi/4\ \varepsilon\ \pi/4)\begin{pmatrix} \sin\frac{\pi}{4} \\ 0 \\ \cos\frac{\pi}{4} \end{pmatrix} = \begin{pmatrix} 1 & 0 & 0 \\ 0 & \cos\varepsilon & \sin\varepsilon \\ 0 & -\sin\varepsilon & \cos\varepsilon \end{pmatrix}\begin{pmatrix} \sin\frac{\pi}{4} \\ 0 \\ \cos\frac{\pi}{4} \end{pmatrix} = \begin{pmatrix} \frac{1}{\sqrt{2}} \\ \frac{1}{\sqrt{2}}\sin\varepsilon \\ \frac{1}{\sqrt{2}}\cos\varepsilon \end{pmatrix} = \mathbf{B}$$

where **D** is the rotation operator as defined in [18] (or, in most texts treating rotations of angular-momentum operators) and **B** is the general vector giving the direction cosines of the gamma beam parallel to the cone surface for various rotation angles, ε. It should be noted that each pair of vectors on the cone surface related by rotation

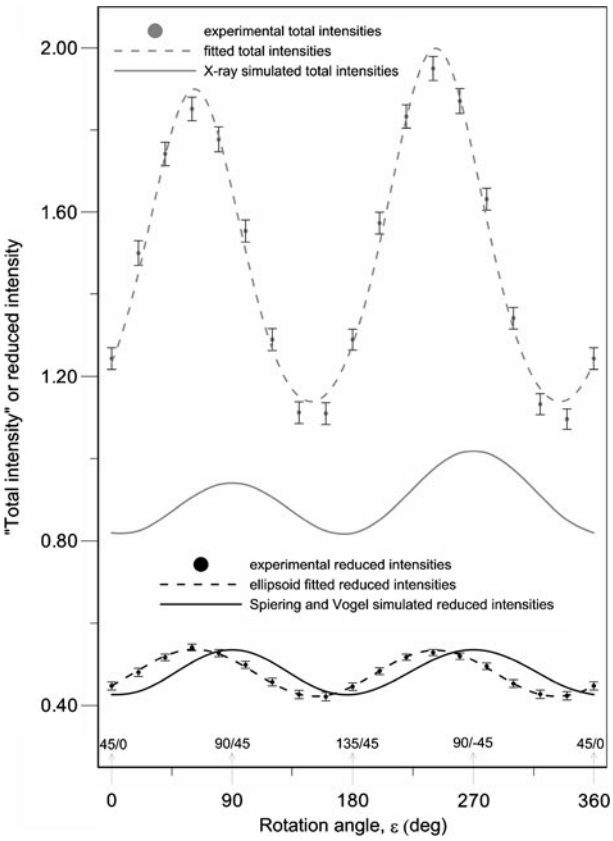

Fig. 2 Calculated and observed reduced and total "intensities": here the "intensities" are actually background-corrected dimensionless areas

angles ε and $\varepsilon + \pi$ are coplanar with the rotation vector, $\mathbf{a}'$. An additional measurement perpendicular to the crystal plate, that is along $\mathbf{a}'$, is required in order to provide sufficient independent orientations to determine the <msd> tensor.

2.3 Intensity calculations

Following Bull et al. [8], we shall simulate the expected reduced intensities, $I^{(r)}$, given by (10)

$$I^{(r)} = I^0_\ell / (I^0_\ell + I^0_r) \tag{10}$$

where I^0_ℓ and I^0_r are respectively the left and right line intensities in the "thin crystal limit" (designated by superscript zero) of a quadrupole doublet over a 2π angular range on the surface of a cone in the crystal traced out by the gamma beam. The intensity calculations are effected by programme MOSREF [19] that utilizes exact (numerical) diagonalizations of the Hamiltonian matrix in arbitrary coordinates and the transition intensity Eq. 20 of Bull et al. [8]. It is useful to clarify further the calculation of total intensities, in this case the sum over two symmetry-related sites.

In MOSREF the intensity normalization over eight hyperfine states between ground and excited states is to unity. Then the total intensity for orientation, i, is from Eqs. 6 and 7

$$\left.\begin{array}{l} f_i \times nsite \times 1 = f_i \times nsite \\ or \\ f_i \times nsite/nsite = f_i \ \ per \ \ site \end{array}\right\} \tag{11}$$

Further details are to be found in references [8, 9]. In this work we utilized, initially, the X-ray-determined <msd> matrix, Eq. 5, and the efg matrix, Eq. 9, obtained from the Spiering and Vogel macroscopic determination [4]. For *one* example from Section 2.1, namely, $P_{xz} = 0$, $P_{yz} = \pm 0.1751$, some of the results are illustrated in Fig. 2. The choice of off-diagonal elements, in principle indeterminate, in this example is not completely arbitrary as will be explained below.

3 Experimental

All Mössbauer (transmission) measurements were carried out at room temperature (295 K) on a PC-based ORTEC multichannel scaling system together with ELSCINT drive electronics operated in constant acceleration mode. A ^{57}Co/Rh source of nominal strength 5 mCi was used as gamma source and a standard iron foil of thickness 12.7 μm was used as the velocity and isomer shift calibrant.

Large single crystals were grown from an aqueous solution of Analar FCL acidified with HCl. A plate of dimensions about 12 mm diameter and thickness 0.7 mm was selected and found, from good 90° extinctions under the polarizing microscope, to be a single crystal. The crystal was super glued to a 0.5 mm thick Perspex disc, mounted in a brass guide and hand polished to a final thickness of 0.138 ± 0.001 mm. The crystal was coated with araldite glue to prevent oxidation during measurements. Expressed as "thickness", t, in units mass total Fe per unit area, we have $t = 7.482$ mg Fe cm^{-2}, or in the 45° orientation 10.581 mg Fe cm^{-2}. The Perspex disc with crystal was then located on a single circle goniometer which was itself mounted at 45° to the gamma-beam direction on a brass collimator with bore diameter 6 mm; the distance from source to the centre of the crystal was 25 mm. The area of crystal exposed to the gamma beam was restricted to a circle of diameter 9 mm by a 0.15 mm thick annular Pb mask; as "seen" by the source this is, of course, an elliptic section. A further Pb mask, with 6 mm aperture, was situated immediately in front of the gas-proportional detector to ensure that the irradiated area of the detector window was greater than the mask aperture for all positions of the source. This set-up ensured that all gamma rays reaching the detector had passed through the crystal and only those gammas from the projected umbra of the source actually reached the detector. We gratefully acknowledge discussions with Dr. Hartmut Spiering, Mainz, on this latter point (WCT, pers. communication).

About 10^6 off-resonance counts were accumulated for each of 20 spectra collected at 20° intervals in the 45° orientation and 2×10^6 off-resonance counts accumulated with the crystal perpendicular to the gamma beam. This latter measurement is important in two respects. Firstly, as already noted, for all rotations by angle ε, the rotation axis is common to all pairs of cone orientations, ε and $\varepsilon + \pi$. Secondly, the measurement along the rotation axis provides an extra dimension to the ellipsoid

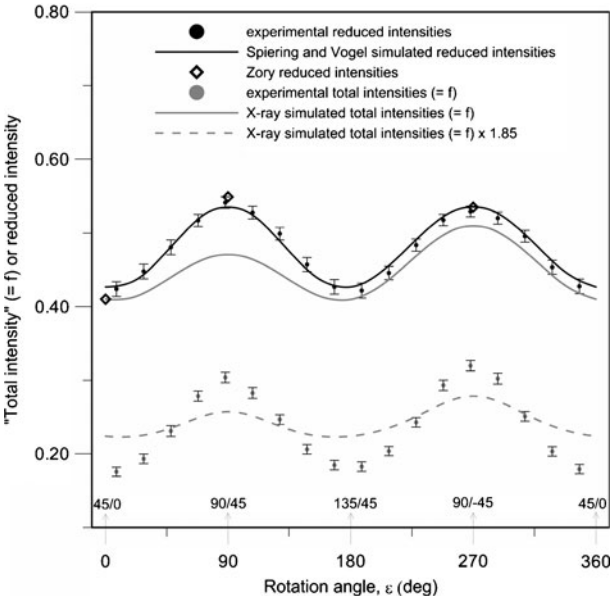

Fig. 3 Calculated and observed reduced intensity and total intensity curves (refer to text for details). The number pairs above the horizontal abscissa are the polar and azimuthal angles corresponding to rotation angles, ε. Points designated by ◇ are taken from Zory [1]

describing the intensity and <msd> tensors (refer to Appendix) and proved crucial, at least in initial fits, in obtaining a good convergence. Spectra were best fitted to Lorentzian line shapes for two quadrupole doublets, one arising from FCL and the second, very weak doublet, arising from an Fe^{3+} impurity (see Section 4 below) using programme MOSFUN [20].

4 Results and discussion

4.1 Preliminary discussion—comparison of calculated and experimental intensity curves

Here we discuss the information that is available, qualitatively or semi quantitatively from Figs. 2 and 3. A couple of representative single crystal FCL Mössbauer spectra in two crystal orientations are given in Fig. 4.

Figure 2 shows a comparison of calculated and observed reduced areas (lower two curves) of the quadrupole doublet lines and, (upper two curves) the total areas as obtained from the Spiering and Vogel [4] macroscopic intensity tensor and X-ray determined msds. The experimental data is based simply on background-corrected dimensionless (Lorentzian) areas. Clearly the functional form of the observed and calculated curves is similar and by shifting the observed curves by rotational angle 28° we can match nicely the maxima and minima of the curves—as is portrayed in Fig. 3. The rotation-angle correction was obtained by comparing least-squares fits of calculated and experimental data. This translation ensures that the Mössbauer data are now well defined in the chosen orthogonal frame, (x_0, y_0, z_0) of Fig. 1.

Figure 2 is, however, not a particularly good way of illustrating the results for total intensities and, in Fig. 3, we show the related curves obtained by dividing the

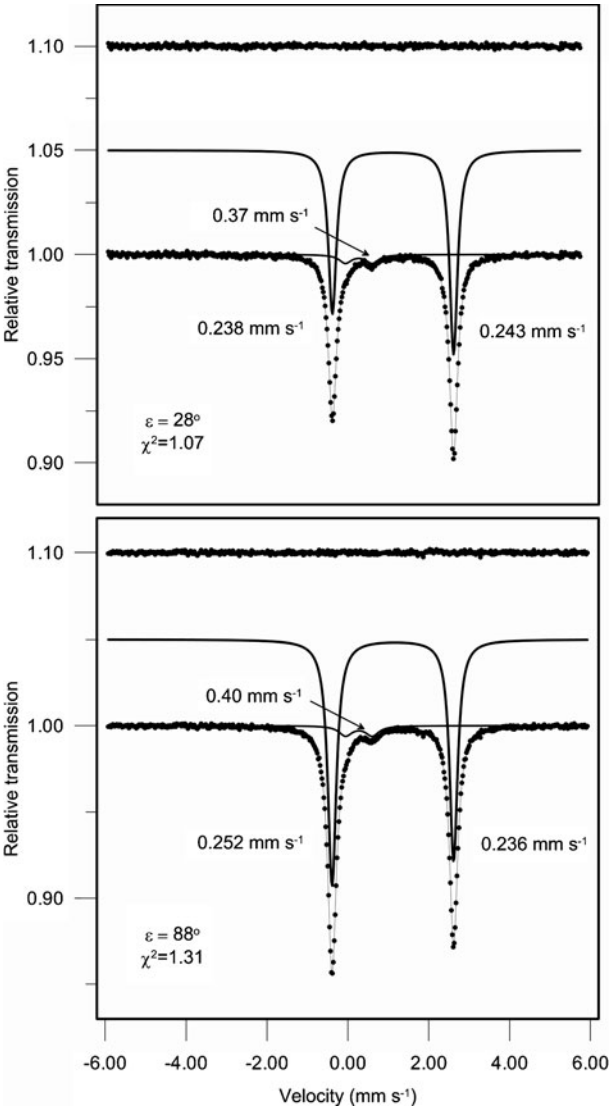

Fig. 4 Representative spectra for FCL showing for each the fitted spectrum, the doublet subspectra and the difference spectrum; χ^2 and line widths are given for each

experimental data of Fig. 2 by the dimensionless quantity $n_{\mathrm{Fe}}\sigma_0$, where n_{Fe} is the number of resonant Fe atoms per unit of area and σ_0 the resonant cross section per Mössbauer nucleus ($= 255.75 \times 10^{-20}$ cm^2 for ^{57}Fe) [21]. (The reduced intensities are not affected by this operation). For our "thin" crystal (thickness, $t = 7.482$ mg Fe cm^{-2} or, in the 45° orientations, 10.581 mg Fe cm^{-2}) the experimentally observed and calculated reduced intensity curves are in good agreement. Hence, in the case of reduced intensities, the "thin-crystal approximation", that neglects thickness and polarization corrections, is quite a good approximation.

For the total "intensities", the experimentally observed quantities clearly conform to the same functional form as the calculated total "intensity" curve. However,

the observed magnitudes bear little relationship to that calculated from X-ray determined <msd> matrix, Eq. 5. In fact, as illustrated in the lowermost curve of Fig. 3, one must multiply the latter <msd> matrix by a factor 1.85 to obtain a semi-quantitative match to the experimentally observed total intensities.

As pointed out in the introduction, we are dealing, in the monoclinic case, with *macroscopic* tensors for *both* efg and <msd>. In both cases, see for example Eq. 7, the *xz* and *yz* components of the tensors are, in principle, indeterminate. There are, however, several relaxations that one might make to modify this rigid statement. For example, we have chosen for the illustration of the efg tensor in Fig. 3 the approximation $P_{xz} \approx 0$. This is based on two additional items of intelligence: (i) the sign of $P_{\hat{z}\hat{z}}$ is positive [1–3] and, (ii) the asymmetry parameter η is small (∼0.1–0.4) [1–3]. (i) and (ii) exclude the approximation $P_{yz} \approx 0$ (when $P_{\hat{z}\hat{z}}$ is positive but $\eta \approx 1$) and the approximation $P_{xz} \approx P_{yz}$ is excluded because $P_{\hat{z}\hat{z}}$ is, in this case, negative. Note that our experiments do *not* determine the sign of $eQP_{\hat{z}\hat{z}}$.

There is also an, apparently sensible, approximation one can make in order to utilize the X-ray determined msds. Let's suppose that the msds appropriate to the Mössbauer experiment differ from those determined by X-ray *only* in respect to their magnitudes and *not* their orientations in the unit cell. Expressed another way we assume as an approximation, that the <msd> matrix, Eq. 3 from X-ray has the same eigenvectors but different eigenvalues to that of the corresponding Mössbauer matrix. The two matrices (tensors) are then related simply by a factor that *is* determinate. This is illustrated for the two total intensity curves of Fig. 3; the X-ray <msd> matrix is multiplied by a factor 1.85 to obtain approximately similar magnitudes in the two curves. From these two curves one can draw the following, interim, conclusions: (i) there is a well-defined angular dependence of the experimental total intensities, (ii) the msds are therefore anisotropic as also are the corresponding absorber recoilless fractions, (iii) taking a mean of experimental total intensity results we obtained f_{abs} (isotropic) = 0.24 in good agreement with the isotropic value, 0.28, as determined by Gibb [3] and assumed by Spiering and Vogel [4] from a powder determination [7] *after* thickness and polarization corrections of their experimental data. We shall expect these conclusions to be modified following thickness and polarization corrections to our data.

4.2 The macroscopic intensity tensor

We shall consider first the evaluation of the macroscopic efg (intensity) tensor, **P**, in the thin-crystal approximation. There are two ways in which this may be achieved, namely, via the refinement options of programme MOSREF [8, 9, 19] or, equivalently, by an algebraic method whereby the reduced intensities are fitted to an ellipsoid expression (see Appendix for detail). The former requires both reduced intensity and total intensity data and returns first estimates of each of the matrices **P** and <**msd**>. For the moment we require only the P matrix and choose therefore to use the ellipsoid procedure. From Appendix, Eq. 25, the fitted macroscopic efg tensor in the intensity tensor formalism is, in the thin-crystal approximation

$$\begin{pmatrix} -0.0846 & 0.0010 & P_{xz} \\ 0.0010 & 0.1559 & P_{yz} \\ P_{xz} & P_{yz} & -0.0713 \end{pmatrix} \tag{12}$$

From Eq. 8, $P_{xz}^2 + P_{yz}^2 = 0.028601$. The result is in good agreement with the Zory [1] and Spiering and Vogel [4], Eq. 9, macroscopic tensors, also in the thin crystal approximation (see again Appendix for details). In the further approximation of Section 2.1, namely, $P_{xz} \approx 0$ we find $P_{yz} = \pm 0.1691$ in fairly good agreement with the value ± 0.17511 and Eq. 9 used in preparing the plots of Figs. 2 and 3.

4.3 Thickness and polarization corrected results

Thickness and polarization corrections of the raw data were effected using the methods outlined in Housley et al. [22] and detailed by Zimmermann [11]. Housley et al. used a series expansion of the theoretical expression for the absorption area of a Mössbauer line due to Bykov and Hein [23]. From Housley et al. [22] and Zimmermann [11] a few terms in the appropriate expression for the area, S, in terms of thickness, p, and fractional polarization, a, and its inversion are, as taken from Bull et al. [8]

$$S = p - \frac{1}{4}(1 + a^2)\, p^2 + \frac{1}{16}(1 + 3a^2)\, p^3 - \frac{5}{384}(1 + 6a^2 + a^4)\, p^4 + \ldots\ldots \tag{13a}$$

and

$$p = S + \frac{1}{4}(1 + a^2)\, S^2 + \frac{1}{16}(1 + a^2 + 2a^4)\, S^3 + \frac{5}{384}(1 + a^4 + 6a^6)\, S^4 + \ldots\ldots \tag{13b}$$

Further terms in the expansions are to be found in Zimmermann [11] and Bull et al. [8]. In the "thin-crystal approximation" referred to in Section 4.1, only the *first* term on the right-hand side of each of Eq. 13a and b is retained. Thickness corrections, with fractional polarizations assumed as zero, affected *both* the reduced intensities (areas) and total intensities (areas). The magnitudes of the corrections ranged from about 7–10%. Fractional polarizations ranged from about 0.25 to 0.38 for the low-velocity line and about 0.23 to 0.50 for the high-velocity line. With fractional polarizations included a further, smaller, correction to both reduced intensities and total intensities followed.

Firstly, we require a thickness correction in the absence of polarization using Eq. 13b with $\alpha = 0$. For our thin FCL crystal a good convergence was obtained with just the four terms of Eq. 13b—as was confirmed by substitution in Eq. 13a. Using the thickness-corrected reduced areas, now termed thicknesses, p_ℓ and p_r, we carried out second parameter refinement with programme MOSREF and obtained for the P and <msd> matrices

$$\mathbf{P} = \begin{pmatrix} -0.0846\,(42) & -0.0009\,(12) & 0 \\ -0.0009\,(12) & 0.1562\,(42) & 0.159\,(17) \\ 0 & 0.159\,(17) & -0.0715\,(19) \end{pmatrix} \tag{14}$$

and

$$\langle \mathbf{msd} \rangle = \begin{pmatrix} 1.4008\,(45) & 0.0261\,(23) & \sim 0 \\ 0.0261\,(23) & 1.0229\,(59) & \sim 0 \\ \sim 0 & \sim 0 & 2.3005\,(109) \end{pmatrix}$$

In this case the principal values of (14) are -0.161, -0.085, 0.246 and $\eta = 0.311$.

Table 1 Results of thickness and polarization iterations; iteration 1 involves thickness correction only—the <msd> matrix is not determined; iterations 2, 3 and 4 include both thickness and polarization corrections

Iteration	Matrix	xx	xy	xz	yy	yz	zz	η/f(iso)
1	**P**	−0.0846	0.0010	0	0.1559	0.1691	−0.0713	0.312
	<**msd**>	–	–	–	–	–	–	–
2	**P**	−0.0847	−0.0009	0	0.1562	0.1689	−0.0715	0.311
	<**msd**>	1.4008	0.0261	0	1.0229	0	2.3005	0.236
3	**P**	−0.0911	−0.0011	0	0.1775	0.1524	−0.0864	0.263
	<**msd**>	1.1962	0.0304	0	0.7009	0	2.1887	0.304
4	**P**	−0.0921	−0.0010	0	0.1789	0.1512	−0.0868	0.255
	<**msd**>	1.2005	0.0329	0	0.6944	0	2.1960	0.304

Table 2 Parameter matrices, **P** (intensity) and <**msd**>, together with their principal values and directions; error estimates are given in parentheses

Y	Parameter matrix, Y			k	Principal values, Y_k	Principal directions[a]	
						θ_k(deg)	ϕ_k(deg)
Matrix **P**	−0.0921 (15)			1	−0.1552 (19)	65.7 (4)	90
	−0.0010 (8)	0.1789 (31)		2	−0.0921 (15)	90	0
	0	0.1512 (48)	−0.0868 (15)	3	0.2473 (65)	24.3 (4)	270
	$\eta = 0.255$ (20)						
Matrix <**msd**>	1.2005 (48)			1	0.6922 (42)	90	93.7 (2)
	0.0329 (15)	0.6944 (42)		2	1.2026 (48)	90	3.7 (2)
	0	0	2.1960 (125)	3	2.1960 (125)	180	–
	f_{abs}(isotropic) = 0.304 (3)						

[a] Angle θ measured from **b** and angle ϕ measured from **a**′ towards –**c**

Utilizing the macroscopic intensity tensor from (14) the new thicknesses including polarization are determined using Eq. 13b. These thicknesses are now designated p_ℓ^0 and p_r^0 and may be identified as the experimental equivalents of I_ℓ^0 and I_r^0 respectively of Eq. 8. New estimates of P and <msd> matrices were obtained from programme MOSREF as above. Two further iterations of this procedure were sufficient to reach convergence. The results are summarized in Table 1. Table 2 details the results for the convergent case, iteration 4 of Table 1. The root-mean-squared deviation (RMSD) between observed and calculated reduced intensities and total intensities for the results in Table 2 is 0.00228 intensity units. In Table 2 the results are given for only one of the two symmetry-related sites, arbitrarily site 1. The corresponding matrices for the second site are obtained from a rotation π about the crystallographic b axis [8]. The microscopic (site) contributions to the fitted macroscopic intensities are shown in Fig. 5.

In the above we have refined the <msd> matrix and, from its eigenvalues, we may obtain, using Eq. 7, the corresponding f_{abs} values as 0.500, 0.300 and 0.111. Alternatively, by virtue of Eq. 11, we can refine an equivalent matrix of f_{abs} values; naturally the eigenvectors and hence the principal directions are identical with those of the <msd> matrix. Since $nsite = 2$, the input total intensities are just $\frac{1}{2}\times$ those

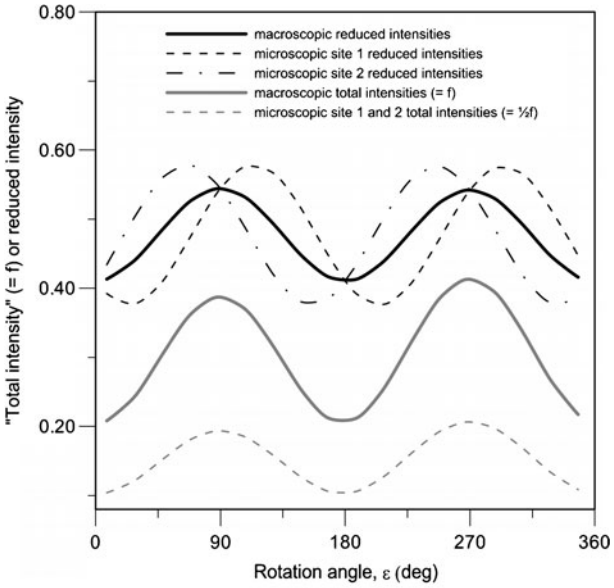

Fig. 5 Calculated microscopic (site) reduced intensity and total intensity curves that average for the former and add for the latter to give the respective fitted macroscopic intensity curves

entered to refine the <msd> matrix. The f_{abs} matrix so obtained, along with error estimates is

$$\mathbf{f}_{abs} = \begin{pmatrix} 0.3012\ (14) & -0.0129\ (6) & 0 \\ -0.0129\ (6) & 0.4496\ (21) & 0 \\ 0 & 0 & 0.1113\ (14) \end{pmatrix} \tag{15}$$

Taking $\frac{1}{3}\times$ the trace of this matrix we obtain the value f_{abs} (isotropic) = 0.3040(25), as given in Table 2, which may be compared with the value 0.28 ± 0.02 obtained by Gibb [3] and the result $f_{powder} = 0.29$ obtained by Kerler and Neuwirth [7].

From Table 2 the following observations are evident. As expected of a low symmetry site, no two P or <msd> principal directions are coaxial (within the combined errors). P_2 and $<msd>_2$ are, however, almost parallel (angle 3.7°) and both lie close to $\mathbf{a}'$ (P_2 parallel and $<msd>_2$ 3.7° away). $<msd>_3$ lies along **b** while $<msd>_1$ lies close (3.7° away) to **c**. Thus the <msd> principal directions lie close to the orthogonal axes that have been chosen as the reference set and, **a** excepted, close to the crystallographic axes; the angle between $<msd>_2$ and **a** is actually quite small also—about 7°. Grant et al. [10], in their study of sodium nitroprusside found also that the msd principal directions lay approximately along the crystallographic axes and commented: "The msd … will be strongly influenced by long wavelength (phonon) vibrations in the crystal which reflect the basic symmetry of the lattice rather than the approximate local symmetry of the iron atoms". The Mössbauer interaction has a finite lifetime of $\sim 0.98\times10^{-9}$ s, while typical phonon vibrational periods are $\sim10^{-12}$ to $\sim10^{-13}$ s, that is, there is sufficient time for the excited Mössbauer state to couple with the long wavelength vibrations. In contrast, X-ray diffraction occurs by a fast scattering process where the interaction period is short compared to phonon

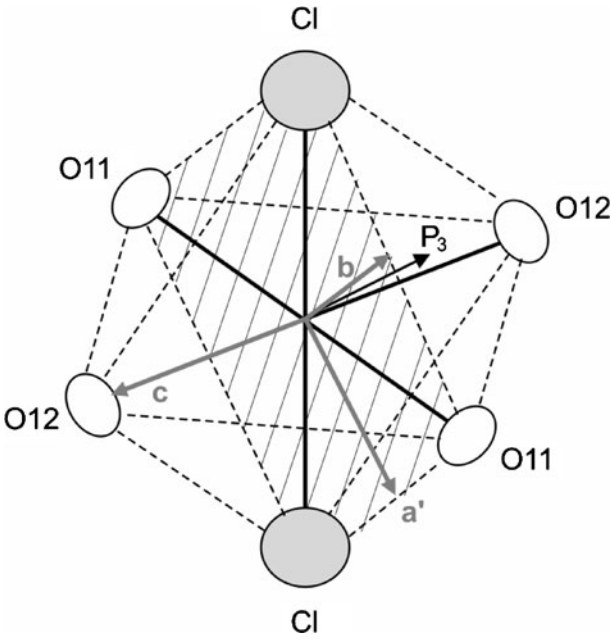

Fig. 6 The FeO_4Cl_2 distorted octahedron showing the relative positions of atoms and orientations of the reference axes. The principal direction of microscopic $P_3 = P_{\hat{z}\hat{z}}$ is shown. All vectors shown are projected to touch the three dimensional octahedron surface

vibrational period. Hence we might expect the msd interaction to reflect rather local symmetry. (Parenthetically, we note that the phonon energies are quantized and any coupling occurring is restricted to particular quantized levels.) These conclusions may need some modification if we relax the restrictions outlined in the final paragraph of Section 2.1 and allow all 11 independent parameters to minimize in the data fitting. We shall discuss this further below.

From Fig. 6 the axes **a**′ and **b** lie in the Cl-Fe-O11 plane and the Fe-O12 bond is parallel to **c**. Since, from Table 2, P_2 lies approximately along **a**′ the other two principal values must, within error, lie in the bc plane: P_3 makes an angle 24.3 with –**c** and P_1 makes an angle 24.3° with the crystallographic monoclinic axis **b**.

The results thus far discussed are in terms of the approximations outlined in the final paragraph of Section 2.1. We need now to relax these restrictions. Allowing all 11 independent parameters of the spin Hamiltonian to minimize, results in a further small (∼2%) diminution of the RMSD. The parameters previously not minimized, namely, P_{xz}, $<msd>_{xz}$ and $<msd>_{yz}$ all take sensibly small values but with errors ranging from 30 to 60% of the magnitude of the parameters. That is, they are certainly not well determined but, apparently, still statistically significant. If, however, the parameters were truly indeterminate, as is generally thought to be the case for Laue site symmetry $\bar{1}$ in a monoclinic crystal, we should have expected the parameters to take on wildly large magnitudes during minimization while having negligible effect on the RMSD. How do these poorly determined parameters affect the conclusions above?

The <msd> matrix principal directions now make angles 5.4°, 5.6° and 6.3° (in the order of smallest to largest) respectively with the reference axes, **c**, **a**′ and **b**. That is, the principal directions are still located, within error, along the crystallographic axes. The largest magnitude msd principal value is 2.227 (equivalent to a mean-squared

displacement of 0.0412×10^{-16} cm^2) implying that, in the Mössbauer experiment at least, the axis along which it lies, to a good approximation the monoclinic unique axis **b**, is an axis of "easy recoil"; the equivalent f_{abs} value is 0.106. As we shall see below this easy-axis-recoil notion is not mirrored in the X-ray determined <msd> matrix.

The results for the P matrix, however, produce uncertainties that are more problematic. An independent determination of the asymmetry parameter would clarify the situation. Zimmermann [2] points out that an independent determination of η from, for example, magnetically perturbed spectra preferably at the same temperature as the non-perturbed experiments would in principle solve the ambiguities that arise from two symmetry-related sites. He also outlines the reasons why, to date, this has not been achieved.

Averaging the two P matrices over the two symmetry-related sites, when $P_{xz} = P_{yz} = 0$ we obtain, since P_{xy} is also (within error) zero, the macroscopic intensity tensor as the diagonal elements of the P matrix of Table 2. In this case, $P_{\hat{z}\hat{z}}$ lies along the crystallographic b axis and the two minor axes lie in the $a'c$ plane and, within error, $P_{\hat{x}\hat{x}}$ is parallel to $\mathbf{a}'$ and $P_{\hat{y}\hat{y}}$ parallel to **c**. These observations are in agreement with those advanced by Zimmermann [11] based on the experimental data of Spiering and Vogel [4]. Taking $\frac{1}{3}\times$ the trace of the <msd> matrix produces $<msd>_{\rm iso} = 1.3636$. If we input the <msd> matrix as the diagonal isotropic matrix with this value and hold it fixed while iterating on the P matrix we obtain the microscopic P matrix in this approximation. Averaging over the two symmetry-related sites, we obtain an estimate of the macroscopic intensity tensor again in the approximation that the <msd> tensor is isotropic. For the microscopic tensor the eigenvalues are −0.169, −0.074 and 0.244 with $\eta = 0.389$. The macroscopic intensity tensor is, as before to a very good approximation diagonal with principal values −0.090, 0.164 and −0.074 in fairly good agreement with those found by Spiering and Vogel (see Eq. 9).

A further useful calculation is to express $P_{\hat{z}\hat{z}} = V_{\hat{z}\hat{z}}$ in SI units, electric potential per unit area in Vm^{-2} as outlined by Zory [1]. Utilizing the well-known formula $\Delta E_Q = \frac{1}{2} e\, Q\, P_{\hat{z}\hat{z}} \left(1 + \frac{\eta^2}{3}\right)^{1/2}$ with $Q = 0.160$ b and, from our current work, $\Delta E_Q = 2.994$ mms^{-1} $= 2.306 \times 10^{-26}$ J and $\eta = 0.255$, we obtain $P_{\hat{z}\hat{z}} = 1.780 \times 10^{14}$ Vm^{-2}. Had we used instead $\Delta E_Q = 2.994$ mms^{-1} $= 2.306 \times 10^{-26}$ J as before but with $\eta = 0.389$ we obtain $P_{\hat{z}\hat{z}} = 1.756 \times 10^{14}$ Vm^{-2}. That is, a ∼50% increase in η results only in a 1% increase in the electric-field gradient.

It is of considerable interest also to reverse our original calculations, namely, to calculate the expected X-ray <msd> matrix from *Mössbauer*-determined ADPs. Utilizing, from Eq. 3, the relationship $U^C_{ij} = \left(1/k^2\right) < msd >_{ij}$ with $k^2 = 53.3494 \times 10^{16}$ cm^{-2} for ^{57}Fe radiation we obtain the following "expected" X-ray <msd> matrix.

$$\mathbf{U}^{\rm C}_{\rm calc} = \begin{pmatrix} 0.02250 & 0.00062 & 0 \\ 0.00062 & 0.01302 & 0 \\ 0 & 0 & 0.04116 \end{pmatrix} \Rightarrow \mathbf{U}^{\rm C}_{f} = \begin{pmatrix} 0.02250 & 0 & 0.00062 \\ 0 & 0.04116 & 0 \\ 0.00062 & 0 & 0.01302 \end{pmatrix} \tag{16}$$

The second matrix in Eq. 16 refers to the expected orthogonalized matrix in the crystal axis system that may be compared to the second matrix, $\mathbf{U}^{\rm C}$, of Eq. 2. Probably

a fairer comparison is the approximation taking the smaller two matrix elements of $\mathbf{U}^{C}$ as zero, namely

$$\begin{pmatrix} 0.00906 & 0.00122 & \sim 0 \\ 0.00122 & 0.01449 & \sim 0 \\ \sim 0 & \sim 0 & 0.00937 \end{pmatrix} \tag{17}$$

with eigenvalues 0.00880, 0.01475 and 0.00937. Comparing the diagonal elements of $\mathbf{U}_f^C$ with these eigenvalues we find the former are, on average a factor of 2.2 larger. This is similar to the ratio observed by Grant et al. [10] for sodium nitroprusside although those authors had only the X-ray isotropic temperature factor for comparison. We note, however, that the ratio for the two largest elements of the matrices is about three and infer that the X-ray msd matrix gives no indication of an "easy" axis of recoil. Considering next principal directions of $\mathbf{U}_f^C$ and Eq. 17, the two largest principal values are approximately parallel (angle 12.1°). The other principal values are also approximately coaxial but in this case the ordering of eigenvalues must be swapped. These observations might go some way to explaining why one is able to use X-ray determined msds to glean useful information on the form of single crystal Mössbauer intensity curves, as evidenced by the plots of Figs. 2 and 3. The predictions are, however, at best, only semi quantitative. Also crude in this instance is the expectation that Mössbauer total intensities would exceed those predicted from X-ray msds by a factor 1.46 (see discussion in the introduction section).

In summary, in contrast to all previous Mössbauer studies, we believe that we have measured with some precision the <msd> tensor and established that it is substantially anisotropic. In consequence the equivalent matrix of absorber recoilless fractions is also anisotropic. With somewhat less precision, it appears that the msd principal values lie along, or close to, the crystallographic axes. The maximum magnitude principal value is very much larger than might be expected from comparable X-ray measurements and, within error, lies along the monoclinic unique axis **b**. The electric-field gradient tensor is also measured precisely, now for the first time, in the presence of anisotropic absorber recoilless fractions. Assuming an isotropic f_{abs} leads to substantially the same (macroscopic) efg tensor as previously determined.

Acknowledgements Mr. R Spiers, Department of Geology is thanked for help with crystal preparation and Prof. Ward Robinson for some of the initial X-ray results. Dr. Hartmut Spiering is thanked for useful comments and discussions. JNB acknowledges gratefully financial support from a Tertiary Education Top Achiever Scholarship. We are particularly grateful to Prof. Peter Zory, Department of Physics University of Florida who made available to us unpublished data from his 1964 (Carnegie Institute) Ph.D. thesis.

Appendix (prepared, in part, from information provided by Prof. Peter Zory)

The analysis of experimental data by the programme MOSREF [19], a numerical, matrix diagonalization least squares procedure, is believed to be both precise and correct. Such a numerical procedure is, however, not always easy to visualize. In this appendix we consider alternative, but equivalent, fitting procedures that rely on being able to write algebraic expressions for both the reduced intensities and total intensities.

Firstly, the reduced intensities: From Zimmermann [2] the experimental quantities $I^{(r)} = I^{(h)}/\left(I^{(h)} + I^{(\ell)}\right)$ from which we eventually obtain the symmetric traceless efg (intensity) tensor may be expressed as

$$I^{(h)}/I^{(tot)} = \sum_{p,q=x,y,z} I_{pq}\mathbf{e}_{\mathrm{p}}\mathbf{e}_{\mathrm{q}} \tag{18}$$

where $\mathbf{e}_{\mathrm{p}}$, $\mathbf{e}_{\mathrm{q}}$ are orthogonal unit vectors and I_{pq} are components of an intensity tensor whose principal values $I^{(h)}_{\hat{p}\,\hat{p}}$ are given by [24]

$$\left.\begin{aligned} I^{(h)}_{\hat{x}\hat{x}} &= \tfrac{1}{2} - \text{sign}\ (V_{\hat{z}\hat{z}})\ (1-\eta)\Big/\left[8\ \left(1+\tfrac{1}{3}\eta^2\right)^{1/2}\right] \\ I^{(h)}_{\hat{y}\hat{y}} &= \tfrac{1}{2} - \text{sign}\ (V_{\hat{z}\hat{z}})\ (1+\eta)\Big/\left[8\ \left(1+\tfrac{1}{3}\eta^2\right)^{1/2}\right] \\ I^{(h)}_{\hat{z}\hat{z}} &= \tfrac{1}{2} - \text{sign}\ (V_{\hat{z}\hat{z}})\ 2\Big/\left[8\ \left(1+\tfrac{1}{3}\eta^2\right)^{1/2}\right] \end{aligned}\right\} \tag{19}$$

Now Eq. 18 is simply the second degree equation of a quadric surface, an ellipsoid in this case that, following Weil et al. [25], can be written more explicitly as

$$I^{(r)}(\xi) = \sum_{i=x,y,z}\ \sum_{j=x,y,z} I_{i\,j}\xi_i\xi_j \tag{20}$$

If the unit vector ξ is expressed in spherical polar coordinates, $\xi = (\sin\theta\cos\phi\ \ \sin\theta\sin\phi\ \ \cos\theta)$ then (20) becomes

$$\begin{aligned} I^{(r)}(\xi) = {} & I_{xx}\sin^2\theta\cos^2\phi + I_{yy}\sin^2\theta\sin^2\phi + I_{zz}\cos^2\theta \\ & + I_{xy}\sin^2\theta\sin 2\phi + I_{xz}\sin 2\theta\cos\phi + I_{yz}\sin 2\theta\sin\phi \end{aligned} \tag{21}$$

If $I^{(r)}(\xi)$ is measured in a small number of orientations from, at least, two distinct crystal planes, we may evaluate the coefficients, I_{pq}. The number of independent coefficients obtainable is, however, for a site of Laue class $\bar{1}$ in a monoclinic crystal only four since the averages of I_{xz} and I_{yz} over the two symmetry related sites are zero.

As an example, Zory [1, 26] measured spectra from seven different crystal cuts. Each crystal plate was 0.254 mm thick and measurements were made perpendicular to specific crystal orientations and area ratios, $A^{(h)}/A^{(\ell)}$, obtained for each. Expressed in the formalism of Eqs. 18 and 19 and in the coordinate frame as defined in Section 2.1 above, the results in the notation $I^{(r)}\left(\theta/\phi\right) = I^{(h)}/I^{(tot)}$ are:

$I^{(r)}\left(0/0\right) = 0.453$; $I^{(r)}\left(\frac{\pi}{2}/0\right) = 0.453$; $I^{(r)}\left(\frac{\pi}{2}/\frac{\pi}{4}\right) = 0.549$; $I^{(r)}\left(\frac{\pi}{2}/-\frac{\pi}{4}\right) = 0.535$; $I^{(r)}\left(\frac{\pi}{2}/\frac{\pi}{2}\right) = 0.629$; $I^{(r)}\left(\frac{\pi}{4}/\frac{\pi}{2}\right) = 0.535$ and $I^{(r)}\left(\frac{\pi}{4}/0\right) = 0.410$. Then, from Eq. 21, after solving a small number of simultaneous equations, we obtain I_{xy} and two values for each of I_{xx}, I_{yy}, I_{zz}. Averaging these latter three pairs and normalizing the calculated trace, 1.507, to 3/2 as required by (19), we obtain the *macroscopic* intensity tensor in the *thin crystal approximation* as

$$\mathbf{I} = \begin{pmatrix} 0.4295 & 0.0070 & I_{xz} \\ 0.0070 & 0.6450 & I_{yz} \\ I_{xz} & I_{yz} & 0.4255 \end{pmatrix} \Rightarrow \begin{pmatrix} -0.0705 & 0.0070 & P_{xz} \\ 0.0070 & 0.1450 & P_{yz} \\ P_{xz} & P_{yz} & -0.0745 \end{pmatrix} \tag{22}$$

The second matrix in (22) is the traceless intensity tensor that we refer to herein as the P matrix, obtained by subtracting 0.5 from the each of the diagonal elements of matrix **I**. Utilizing the invariant, Eq. 7, it is found that $P_{xz}^2 + P_{yz}^2 = 0.03114$ which is very close to that obtained in the Spiering and Vogel work [4].

A similar procedure is applicable with the angular rotation data of the present work where, for our crystal plane, it is convenient to consider, from Section 2.2, the groups of three coplanar vectors, two on the cone surface related by rotation angles ε and $\varepsilon + \pi$ together with the rotation vector $\mathbf{a}'$ that is coplanar with and common to all such pairs. Then it is shown easily that

$$I^{(r)}(\varepsilon) + I^{(r)}(\varepsilon + \pi) = 2\left\{I^{(r)}\left(\mathbf{a}'\right)\sin^2\theta\cos^2\phi + I_{yy}\sin^2\theta\sin^2\phi + I_{zz}\cos^2\theta\right\} \quad (23)$$

$$I^{(r)}(\varepsilon) - I^{(r)}(\varepsilon + \pi) = 2\left\{I_{xy}\sin^2\theta\sin 2\phi\right\} \quad (24)$$

Equation 23 together with the relationship $I_{xx} + I_{yy} + I_{zz} = {}^3/_2$ produce immediately values of I_{xx}, I_{yy} and I_{zz}, and I_{xy} is obtained from Eq. 24. For our 360-degree rotations we obtain 10 such sets of solutions that can then be averaged. Alternatively, and more generally, we can find the best-fit I_{ij} coefficients of (21) by minimizing the quantity $\left\{I^{(r)}(obs) - I^{(r)}(calc)\right\}^2$ with a suitable least-squares fitting programmme—MINPACK [27] for example. This latter procedure produces

$$\mathbf{I} = \begin{pmatrix} 0.4154 & 0.0010 & I_{xz} \\ 0.0010 & 0.6559 & I_{yz} \\ I_{xz} & I_{yz} & 0.4287 \end{pmatrix} \Rightarrow \begin{pmatrix} -0.0846 & 0.0010 & P_{xz} \\ 0.0010 & 0.1559 & P_{yz} \\ P_{xz} & P_{yz} & -0.0713 \end{pmatrix} \quad (25)$$

with an RMSD of 0.00299 and, $P_{xz}^2 + P_{yz}^2 = 0.028601$ in good agreement with the result obtained from Eq. 22 for the Zory work. The good agreement with the Zory values should not surprise since the crystals used were of comparable thicknesses: 0.254 mm for the Zory slices and, in 45° orientation, 0.195 mm for our experiments. The second matrix in (25) contains the initial values of P elements used in the refinements described in the text.

In the case of the total intensities a functional form is obtained from the theory of X-ray scattering [28, 29] and, for a single-circle goniometer rotation with respect to a calibrated angle, ε, we may write

$$f = A\exp\left\{\sin^2(C\varepsilon)\right\} + B \quad (26)$$

where ε is the goniometer rotation angle and A, B, C are adjustable parameters. When C = 0.5, this functional form can be fitted in excellent accord ($R^2 = 0.944$) with previously published ferrous ammonium sulphate hexahydrate total intensities [8], where the factor of C = 0.5 effectively halves the periodicity of a standard trigonometric function due to the close coaxiality (within experimental error) of the crystallographically unique axis **b** with the goniometer rotation axis. For FCL, the fitting is slightly more complicated, since Eq. 26 would yield a symmetrical double-peak total intensity fit. Experimentally, a small asymmetry between the two total intensity peaks was observed. In turn, the double peak intensity pattern can again be traced back to the physical orientation of the crystal, where for FCL,

the crystallographic unique axis **b** is in the plane of the crystal that is orthogonal to the goniometer rotation axis. The required fitting function therefore contains a trigonometric weighting function applied to two symmetrical functions, giving the expression

$$I^{(tot)} = \left(A \exp\left\{\sin^2(\varepsilon)\right\} + B\right)\left(\frac{1}{2}\sin(\varepsilon) + \frac{1}{2}\right) + \left(C \exp\left\{\sin^2(\varepsilon)\right\} + D\right)\left(\frac{1}{2}\sin(\varepsilon + 180) + \frac{1}{2}\right) \quad (27)$$

where ε is the goniometer rotation angle and A, B, C, D are adjustable parameters, and 180° is the fitted double-peak offset. When this function is fitted to the raw experimental total intensities, the factor of $R^2 = 0.997$ (equivalent to an RMSD of 0.005 intensity units) is obtained, with $A = 0.1478$; $B = 0.2055$; $C = 0.1638$ and $D = 0.1989$. Substitution allows calculation of fitted total intensities for a given ε measurement in the case where the bc plane normal is inclined at 45° with respect to the radiation propagation axis.

References

1. Zory, P.: Phys. Rev. **140**, A1401 (1965)
2. Zimmermann, R.: Nucl. Instrum. Methods **128**, 537 (1975)
3. Gibb, T.C.: Chem. Phys. **7**, 449 (1975)
4. Spiering, H., Vogel, H.: Hyperfine Interact. **3**, 221 (1977)
5. Grant, R.W., Wiedersich, H., Muir, A.H., Gonser, U., Delgass, W.N.: J. Chem. Phys. **45**, 1015 (1966)
6. Ono, K., Shinohara, M., Ito, A., Fujita, T., Ishigaki, A.: J. Appl. Phys. **39**, 1126 (1968)
7. Kerler, W., Neuwirth, W.: Z. Phys. **167**, 176 (1962)
8. Bull, J.N., Robinson, W.T., Tennant, W.C.: Hyperfine Interact. **194**, 347 (2009)
9. Tennant, W.C.: J. Phys., Condens. Matter **4**, 6993 (1992)
10. Grant, R.W., Housley, R.M., Gonser, U.: Phys. Rev. **178**, 523–530 (1969)
11. Zimmermann, R.: In: Thosar, B.V., Srivastava, J.K., Iyengar, P.K., Bhargava, S.C. (eds.) Advances in Mössbauer Spectroscopy, pp. 273–315. Elsevier, Amsterdam (1983)
12. Penfold, B.R., Grigor, J.A.: Acta Crystallogr. **12**, 850 (1959)
13. Meunier-Piret, P.J., Van Meersche, M.: Acta Crystallogr. B **28**, 2329 (1972)
14. Verbist, J.J., Hamilton, W.C., Koetzle, T.F., Lehmann, M.S.: J. Chem. Phys. **56**, 3254 (1972)
15. Bull, J.N., Fitchett, C.M., Maclagan, R.G.A.R., Tennant, W.C.: J. Phys. Chem. Solids **71**, 1746 (2010). doi:10.1016/j.jpcs.2010.09.009
16. Trueblood, K.N., Bürgi, H.–B., Burzlaff, H., Dunitz, J.D., Gramaccioli, C.M., Schulz, H.H., Shmueli, U., Abrahams, S.C.: Acta Crystallogr. **A52**, 770 (1996)
17. Johnson, C.K.: A Fortran thermal ellipsoid plot program for crystal structure illustrations. ORNL Report No. 3794. Oak Ridge National Laboratory, Oak Ridge (1965)
18. Golding, R.M., Tennant, W.C.: Quantum mechanics in chemical physics: an exploration. Common Ground Publishing, Melbourne (2008)
19. Tennant, W.C., McGavin, D.G., Patterson, K.H.: New Zealand Institute for Industrial Research, IRL Report No. 8 (1992)
20. Müller, E.W.: Mössbauer spectrum fitting program for universal theories. Institut für anorganische Chemie und analytische Chemie, Johannes Gutenberg Universität, Mainz (1980)
21. Gütlich, P., Link, R., Trautwein, A.: Mössbauer spectroscopy and transition metal chemistry. Springer, Berlin (1978)
22. Housley, R.M., Grant, R.W., Gonser, U.: Phys. Rev. **178**, 523 (1969)
23. Bykov, G.A., Hien, P.Z.: Sov. Phys. JETP **16**, 646 (1963)

24. Wegener, H.H.F., Obenshain, F.E.: Z. Phys. **163**, 17 (1961)
25. Weil, J.A., Buch, T., Clapp, J.E.: Adv. Magn. Reson. **6**, 183 (1973)
26. Zory, P.: Ph.D. thesis, Department of Physics, Carnegie Institute of Technology (unpublished) (1964)
27. Moré, J.J., Garbow, B.S., Hillstrom, K.E.: User guide for MINPACK Argonne National Laboratory. Argonne, IL, USA (1980)
28. Shapiro, F.L.: Usp. Fiziol. Nauk **72**, 684 (1960)
29. Danon, J.: Lectures on the Mössbauer effect, pp. 8–13. Gordon and Breach, Scientific Publishers, Inc., New York (1968)